RESEARCH ARTICLE
doi: 10.2306/scienceasia1513-1874.2025.031

ScienceAsia 51 (2): 2025: ID 2025031: **1**–**12**

Effect of temperature of boric acid-doped porous activated carbon preparation on the electrochemical capacitor performance

Tawatchai Kangkamano[a], **Panita Kongsune**[a,b,*], **Kantrakorn Suwanraksa**[a], **Tantika Charoenlap**[a], **Sirikorn khaophong**[a], **Sonchai Intachai**[a,b]

[a] Department of Chemistry, Faculty of Science and Digital Innovation, Thaksin University, Phattalung 93210 Thailand
[b] Innovative Material Chemistry for Environment Center, Thaksin University, Phattalung 93210 Thailand

*Corresponding author, e-mail: dpanita@tsu.ac.th

Received 20 May 2024, Accepted 23 Feb 2025
Available online 1 May 2025

ABSTRACT: This research aims to utilize coffee grounds as a sustainable precursor for activated carbon preparation, varying carbonization temperature and activator concentration and enhancing its electrochemical performance through boric acid doping. Coffee grounds, KOH, and water were mixed in weight ratios of 1:0.5:2 and 1:1.0:2, stirred, incubated at room temperature for 24 h, and then carbonized in a furnace at 400, 500, 600, and 700 °C for 4 h. Structural, morphological, and chemical properties of the optimal conditions of AC0.5_500, AC1.0_500, AC0.5_600, and AC1.0_600 revealed evenly distributed pores, higher surface area, graphitization, and yield percentage. Subsequently, four selected samples underwent surface treatment with boric acid at 140 °C for 48 h via hydrothermal treatment. Electrocapacitive behavior was investigated, revealing that among the different temperatures and activating contents in both doping and undoping samples, higher temperatures and KOH content induced higher specific capacitance values. As a result, B_AC1.0_600 exhibited good electrochemical behavior with a capacitance of approximately 282 $\mathrm{F \cdot g^{-1}}$, an energy density of 16.54 $\mathrm{Wh \cdot kg^{-1}}$, and a power density of 138.54 $\mathrm{W \cdot kg^{-1}}$ at a current density of 0.5 $\mathrm{A \cdot g^{-1}}$. These findings suggest that porous carbons derived from waste coffee grounds and modified with boric acid hold significant potential as alternative electrode materials for supercapacitors.

KEYWORDS: activated carbon, coffee grounds, carbon electrode, boric acid

INTRODUCTION

In the pursuit of sustainable and eco-friendly energy storage solutions, advanced material synthesis plays a pivotal role. Electrochemical capacitors, or supercapacitors, are promising for efficient energy storage and rapid release. Generally, supercapacitors can be divided into electrical double layer capacitors (EDLCs) and pseudocapacitors (PCs) [1,2]. PCs store energy based on reversible faradaic reactions on the surface of active materials, while EDL store energy through the electrostatic separation of charges at the electrode-electrolyte interface on the surface and beside pore [3]. The performance of supercapacitors relies heavily on the superficial and porous characteristics of electrode materials [3,4]. The significant correlation between the porous structure of carbon materials and the electrochemical capacitors is vital. Energy storage through this mechanism depends on ions at the electrode/electrolyte interface [3,5]. Therefore, a carbon electrode surface facilitating higher ion retention enhances energy storage capacity. The design of high-performance electrode materials is crucial for fabricating high-energy supercapacitors.

The electrodes of supercapacitors play a crucial role in the performance and characteristics of these energy storage devices. In essence, a greater surface area or sponge-like porous carbon augments the performance of carbon materials for electrode in supercapacitor applications [5–7]. The electrodes are typically made of carbon material or other porous carbon materials, providing a large surface area for the formation of an electric double layer and a greater number of charge carriers [8]. Carbon nanostructures are ideal for supercapacitor fabrication due to their excellent electrical conductivity. However, their synthesis is costly. Hence, there is a need to explore sustainable and inexpensive raw materials for versatile carbon material production along with simple synthesis techniques like activated carbon synthesis [8,9]. Activated carbon also exhibits remarkably high specific capacitance ranging between 100 to 350 $\mathrm{F \cdot g^{-1}}$ [5,10]

One advantage of synthesizing activated carbon is its derivation from biomass precursors through pyrolytic processes at high temperatures and subsequent physical or chemical activation [11,12]. Utilizing waste materials as precursors not only addresses waste management issues but also aligns with sustainability principles. Various methods, including chemical treatments and thermal activation, enhance surface area and charge storage capabilities. Activated carbon can be obtained from diverse sources such as agricultural, industrial, and household waste as well as invasive algae/aquatic plants [1,13]. For instance, coffee grounds, an abundant byproduct of the coffee industry, possess inherent carbonaceous properties suitable for activated carbon preparation [14–16]. Chiu and Lin experimented with various activating agents such as KOH, NaOH, HCl, H_3PO_4, $ZnCl_2$, and $FeCl_3$, finding that KOH-activated carbon electrodes exhibited the highest specific capacitance at 105.3 $F \cdot g^{-1}$ [16]. The activation mechanism of KOH involves the reaction: 4KOH + C <—> 4K + CO_2 + $2\,H_2O$, leading to pore formation as CO_2 gas escapes [17]. Martínez et al [8] synthesized activated carbon from spent coffee grounds using KOH as the activating agent, observing specific capacitances around 205 $F \cdot {}^{g\text{-}1}$ with oxidative calcination and approximately 82 $F \cdot g^{-1}$ with carbonization in an argon atmosphere. Rufford et al [18] studied the effect of mesopores on double-layer capacitance by preparing activated carbon from waste coffee grounds, achieving specific capacitances exceeding 100 $F \cdot g^{-1}$ at fast charge–discharge rates.

Capacitance based on the electric-double layer mechanism may reach its limit despite finely tunable porous structures and surface areas. Recent efforts to enhance the specific capacitance (C_p) of supercapacitors focus on incorporating heteroatoms (e.g., sulfur (S), nitrogen (N), and phosphorus (P)) into porous carbon (C). Oxygen and nitrogen atoms, serving as n-type doping sites, increase electron density in the carbon matrix, enhancing electronic conductivity and surface wettability. For instance, Hegazy et al [19] utilized asphaltene for supercapacitors by doping carbon with P, N, and S using diammonium hydrogen phosphate. Cheng and Wu demonstrated that regenerated nylon 6, a waste nitrogenous polymer, is an excellent precursor for N-doped porous carbon [20]. Boron (B), as a p-type dopant, enhances capacitance; Govindarasu et al [21] showcased boron-doped 3D cubic ordered mesoporous carbon's high specific capacitance and cycling stability. Activated carbon derived from olive stones and coated with silica is promising for supercapacitor electrodes [22]. Ning et al [23] introduced succulent-leaf-derived carbon material with hierarchical porosity and N-S co-doping. Li et al [24] reported N and B co-doped hierarchical porous carbon with excellent electrochemical efficiency. Composite activated carbon with boron exhibits high specific capacitance and specific energy [21, 25]. Increasing capacitance through heteroatom doping is a key method to enhance supercapacitor energy density with exploration into synergistic effects among heteroatoms being an important avenue for research. The heteroatom-doping not only increases pseudocapacitance but also boosts EDL capacitance [25].

This research aims to harness the potential of coffee grounds as a sustainable precursor while enhancing the electrochemical performance of activated carbon through the introduction of boric acid as a dopant. Boric acid (H_3BO_3) introduced both boron and oxygen atoms which increase hydrophilicity and conductivity, leading to enhanced specific capacitance and rate performance. Despite notable progress in doped activated carbon (Dope-AC), the carbonization temperature and activator concentration have often been overlooked and rarely investigated. Therefore, this research explores the effect of temperature and activator amount on the electrochemical capacitor performance of boric acid-doped sponge-like porous activated carbon prepared from coffee grounds. The study presents a detailed synthesis methodology, structural characterization, and evaluation of electrochemical performance. The outcomes contribute to the development of efficient and environmentally friendly electrochemical capacitors.

MATERIALS AND METHODS

Chemical and reagents

The coffee grounds were sourced from a Thaksina café shop in Thaksin University, Phatthalung Province, Thailand. Most chemicals came from Elago Enterprises Pty. Ltd. (Cherrybrook, Australia). The Nafion™117 solution obtained from Sigma-Aldrich Pty. Ltd. (MO, USA).

Preparation of porous activated carbons (ACs)

The coffee grounds were initially dried at 100 °C for 12 h and then crushed into a powder. Next, the fine powders, KOH, and deionized water were combined in mass ratios of 1.0:0.5:2.5 and 1.0:1.0:2.5, respectively, and soaked for 12 h. The resulting mixture was carbonized under atmospheric conditions in a furnace at 400, 500, 600, and 700 °C with a heating rate of 5 °C min^{-1} for 4 h. Afterward, the obtained sample was rinsed with HNO_3 and deionized water until the rinse water reached a neutral pH. Finally, the samples were dried at 100 °C for 24 h. The respective names assigned to the samples were AC0.5_400, AC1.0_400, AC0.5_500, AC1.0_500, AC0.5_600, AC1.0_600, AC0.5_700, and AC1.0_700.

Preparation of boric acid-doped porous ACs

To prepare the modified-boric acid ACs, the selected AC powder (AC0.5_500, AC1.0_500, AC0.5_600, and AC1.0_600) were mixed with 8.5% W/V boric acid (H_3BO_3) at a mass/volume ratio of 4.5:100. The mixtures were stirred and heated at 60 °C for 30 min, followed by sonicating the suspension for 30 min. Subsequently, the resulting mixtures were transferred to a Teflon-lined stainless-steel reactor and treated at 150 °C for 48 h. Afterward, the obtained samples were rinsed with NaOH and deionized water until the rinse water reached a neutral pH. Finally, the samples were dried at 100 °C for 24 h. The prepared samples were named B_AC0.5_500, B_AC1.0_500, B_AC0.5_600, and B_AC1.0_600.

Characterization of boric acid-doped porous ACs

To estimate the surface acidity, 0.20 g of each sample was mixed with 25 cm^3 of 0.05 M NaOH solution in a conical flask and left for 48 h at room temperature. The mixtures were then separated, and the filtrates were titrated using 0.05 M HCl solution. Similarly, to obtain the surface basicity, 0.20 g of each adsorbent was mixed with 25 cm^3 of 0.05 M HCl solution and left for 48 h. The titration solution used in this case was 0.05 M NaOH. The zeta potential value of the samples was conducted using a Zetasizer (SZ-100-HORIBA, Kyoto, Japan). The morphology of the samples was examined using a FEI ESEM Quanta 450 FEG (Hillsboro, Oregon, USA). Elemental mapping and distribution were obtained using Energy Dispersive Spectroscopy (EDS; Merlin compact, Oxford Instruments, Abingdon, UK). Surface functional groups were investigated using an FTIR Spectrometer (ATR-FTIR; G8044AA, Agilent Technologies, Santa Clara, CA, USA) within the range of 650–4000 cm^{-1}. The porous texture of the activated carbons was characterized using N_2 adsorption/desorption isotherms at 77 K, measured with a nitrogen sorption instrument (Quantachrome Autosorb-iQ2-MP, USA). Surface area was determined via the BET (Brunauer-Emmet-Teller) method, and pore size distribution was obtained using the BJH (Barrett-Joyner-Halenda) method. Phase structure verification was conducted through Powder X-ray diffraction (XRD) analysis, utilizing a Bruker D8 ADVANCE diffractometer (Bruker, Billerica, USA) and a PANalytical Empyrean powder diffractometer (Malvern Panalytical, Almelo, The Netherlands).

Electrode preparation and electrochemical measurement

The working electrodes were prepared by mixing AC/dopped-AC samples (0.005 g), 5% (w/v) Nafion solution (0.05 ml), 99% (V/V) isopropanol (0.660 ml), and deionized (DI) water (0.290 ml). This mixture was then coated onto a glassy carbon electrode (GC) with a geometric surface area of 0.0707 cm^2 and dried in an oven at 50 °C for 1 h. The electrochemical performance of the ACs materials was evaluated using a three-electrode cell and an Autolab electrochemical workstation (Metrohm PGSTAT101, Switzerland). An Ag/AgCl electrode was used as the reference electrode, while a Pt wire served as the counter electrode. A 1 M KOH solution was used as the electrolyte. Cyclic voltammetry (CV) measurements were conducted at various scan rates and voltage ranging from 0.05 to 0.125 $V\cdot s^{-1}$ and 0.1 to 0.5 V. The voltage window for both CV and galvanostatic charge-discharge (GCD) measurements was set between −0.2 and 0.4 V, with the current density for GCD measurements ranging from 0.5 to 1.25 $A\cdot g^{-1}$.

RESULTS AND DISCUSSION

Morphological features and composition of ACs and boric acid-doped ACs

SEM micrographs in Fig. 1 depict various surface morphologies of different AC samples (AC0.5_400, AC1.0_400, AC0.5_500, AC1.0_500, AC0.5_600, AC1.0_600, AC0.5_700, and AC1.0_700), resulting from differing chemical activation amounts and temperature treatments. AC0.5_400, activated with a 0.5:1 KOH to coffee ground ratio at 400 °C, exhibits fewer surface pores. Increasing the carbonization temperature to 500 °C (AC0.5_500) under the same activation ratio yields similar surface morphologies. Conversely, higher chemical activation (AC1.0_400 and AC1.0_500) results in surfaces with more pores across both carbonization temperatures. Furthermore, higher carbonization temperatures (AC0.5_600 and AC0.5_700) result in an increased presence of micro/mesopores across their surfaces. Notably, samples subjected to high chemical activation and carbonization temperatures (AC1.0_600 and AC1.0_700) exhibit abundant micro/mesopores. This porous structure, typical in carbons activated with higher KOH ratios and elevated carbonization temperatures, arises from chemical interactions between the reagent and precursor surface, facilitating electrolyte transport during charging/discharging and thereby enhancing electrochemical performance. The percent yield varies significantly across the samples, ranging from 20.19% to 67.36% (Table 1). Increased carbonization temperatures and KOH activation amounts led to decreased yield percentages. Given the crucial role of yield percentage in activated carbon production, AC0.5_500, AC1.0_500, AC0.5_600, and AC1.0_600, characterized by increased graphitization as well as abundant mesopores and micropores, were selected to study the impact of boric acid-doped AC.

Carbon atoms and heteroatoms (oxygen, nitrogen, and boron) play a pivotal role in the organized structure, aromatization, and surface behaviors of activated carbon. The results of elemental analysis for 7 samples are presented in Table 1. EDS data revealed an increase in carbon content for the more KOH-activated and higher carbonization temperature samples, accompanied by a decrease in oxygen content. This led to increased graphitization and removal of volatile compounds after KOH activation and carbonization [12]. In contrast, boric acid (HBO_3) modification on the AC surface (B_AC1.0_600) resulted in a dominant increase in boron and oxygen contents. It is noteworthy that boric acid modification successfully led to the incorporation of oxygen and boron on the AC surface.

Boehm titration of ACs and boric acid-doped ACs

As previously mentioned, oxygen, nitrogen, and boron atoms are pivotal factors influencing the surface properties of activated carbon. The conductive behavior

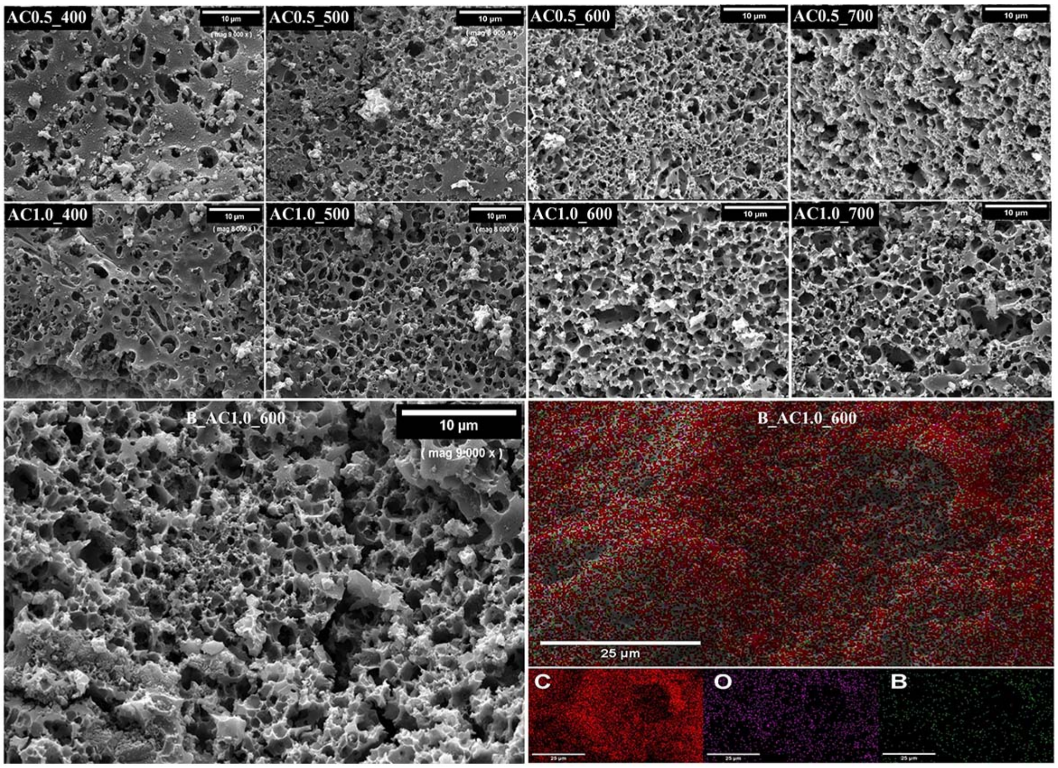

Fig. 1 SEM images of AC0.5_400, AC1.0_400, AC0.5_500, AC1.0_500, AC0.5_600, AC1.0_600, AC0.5_700, AC1.0_700, and B_AC1.0_600, along with the elemental mapping of B_AC1.0_600, showing the distribution of carbon (C), oxygen (O), and boron (B).

Table 1 The element analysis by EDS, basic and acidic sites by Boehm titration, and percent yield of samples.

Sample	% Atomic					Basic site	Acidic site	% Yield
	C	O	B	N	others	(mmol · g^{-1})	(mmol · g^{-1})	
CG	76.41	21.08	–	2.25	0.26	0.9	1.63	–
AC0.5_400	73.35	18.99	–	4.25	3.41	1.04	1.33	67.36
AC1.0_400	75.55	17.65	–	4.33	2.47	1.11	1.21	64.85
AC0.5_500	78.23	16.48	–	4.31	0.63	1.13	1.07	63.60
AC1.0_500	81.02	13.38	–	4.01	1.53	1.38	0.92	61.67
AC0.5_600	79.63	14.63	–	5.37	0.29	1.37	0.93	57.20
AC1.0_600	84.66	8.57		5.97	0.80	1.55	0.85	42.83
AC0.5_700	85.01	9.47	–	5.19	0.29	1.58	0.87	27.24
AC1.0_700	87.49	8.91	–	3.22	1.1	1.54	0.85	20.19
B_AC0.5_500	74.86	15.68	3.18	6.09	0.19	1.59	1.09	–
B_AC1.0_500	75.87	15.11	3.83	4.90	0.29	1.62	1.04	–
B_AC0.5_600	80.30	10.20	4.86	4.51	0.13	1.50	1.01	–
B_AC1.0_600	82.70	10.31	5.79	3.89	0.22	1.53	0.99	–

of the AC electrode can be manipulated through the modification of surface groups. Higher oxygen content renders the surface more acidic, while higher nitrogen content makes it more basic [11]. The acidic and basic surface functionalities are determined through Boehm titration and summarized in Table 1. The values of basic and acidic sites vary across the samples, indicating differences in their chemical properties especially oxygen and nitrogen. The total surface of raw material coffee grounds is more acidic than basic because of its high percentage of atomic oxygen atom. However, AC samples are more basic than acidic when temperature increases, owing to the reduction in oxygen content. Additionally, the basic group value of the boric acid sample is slightly lower than that of the AC sample, signifying that the modification process increased the presence of boron and oxygen-containing groups on the surface of the AC. This result agrees well with the EDS result. Therefore, the temperature and activating agent impacts the enhancement of the surface area and pore development, and the modification of surface agent influences the arrangement of surface functional groups.

SEM images of boric acid doping (B_AC0.1_600) in the activated carbon matrix are presented in Fig. 1. Doping the heteroatom into the activated carbon matrix, the SEM image displays a random pore distribution in the AC sample. The intra-pore space within the carbon material is expected to enhance the electrolyte accessibility ratio. This augmentation fosters both intra- and inter-particle conductivity, leading to an increase in specific surface area and surface wettability. As a result, rapid ion transport is facilitated within the pores. Additionally, the introduction of heteroatoms such as O, N, and B atoms modifies the physical, chemical, and electrochemical properties of the AC, effectively enhancing conductivity. To further confirm the presence of elements in B_AC0.1_600 system, SEM elemental mapping analysis was performed, as depicted in Fig. 1. The mapping image clearly reveals a uniform distribution of individual components C, O, and B. The presence of carbon, oxygen, nitrogen, and boron in the material is further validated by EDX data, as shown in Table 1.

FTIR, BET, XRD, and zeta potential of ACs and boric acid-doped ACs

The conductivity efficiency of AC depends not only on its pore structure but also on the chemical nature of its surface. Various atoms such as oxygen, hydrogen, nitrogen, boron, and others exist as single atoms or in the form of functional groups on the AC surface, potentially enhancing the affinity between the material surface and electrolyte ions. The functional groups on the surface were analyzed using the FT-IR technique, and the FTIR spectra of coffee grounds (CG), coffee grounds activated carbon (AC1.0_600), and boric acid-doped coffee grounds activated carbon (B_1.0AC_600) are displayed in Fig. 2a. In the CG sample, bands at 3360, 2925, 2890, 1741, 1638, 1455, 1240, 1151, 1055, 871, and 807 cm^{-1} were assigned to functional groups such as hydroxyls, phenols, olefins, esters, and ethers. After the thermal-KOH chemical treatment process, the AC1.0_600 sample exhibited broad symmetrical peaks corresponding to C=C and C=O functional groups, indicating a high degree of graphitization.

Upon doping the boric acid (B_AC1.0_600) molecule into the activated carbon matrix, their spectra are quite similar, showing an increased presence of C—O/C—OH, C=O, O—C=O and C—N functional groups, in which the carbonyl group is electrochemically more active. The hydrophilic nature of C—O/C—OH, C=O, O—C=O, and N—C=O functional groups contributes to improved electrode wettability, facilitating the diffusion and movement of electrolyte ions through micropores. The abundance of oxygen-containing functional groups enhances wettability in aqueous electrolytes, fostering stronger affinity between the material surface and electrolyte ions [24]. Consequently, the presence of B—C bonds in boron-doped activated carbon is evident at 1020 cm^{-1} [26] when compared to the infrared spectra of activated carbon, indicating that boron atoms have been successfully intercalated into the carbon matrix of doped porous carbon materials (B_AC1.0_600). This result agrees well with the EDS and the surface acidic and basic sample results.

The nitrogen adsorption/desorption isotherm for GC, AC1.0_600, and B_AC1.0_600 is depicted in Fig. 2b. These isotherms exhibit a similar shape, resembling Type I and IV isotherms, suggesting a mixture of microporous and mesoporous structures. The total specific surface area (SSA) evaluated using the Brunauer-Emmett-Teller (BET) equation for GC, AC1.0_600, and B_AC1.0_600 as shown in Table 2 were 2.31, 470.61, and 305.68 $m^2 \cdot g^{-1}$, respectively. The boric acid-doped AC exhibited a slight decrease in SSA due to the small size of boric acid molecules covering on the AC surface. The observed decline in pore volume is more pronounced in doped activated carbons obtained by boric acid, resulting in a slight decrease in pore size from 2.4 nm to 2.2 nm, as shown in Table 2. This effect is attributed to the blocking of micropores by functional groups (e.g., O and B-doped carbon), preventing N_2 molecule diffusion, consistent with previous reports [19]. With a hydration sphere radius of 0.331 nm for K^+ ions [27], it was found that the diffusion of K^+ electrolyte ions in KOH electrolyte was facilitated by sufficiently micropore sizes.

Table 2 BET surface area, pore volume, pore diameter, and C_p calculated from CV of ACs and B_ ACs.

Sample	BET surface area ($m^2 \cdot g^{-1}$)	Pore volume ($cm^3 \cdot g^{-1}$)	Pore diameter (nm)	C_p ($F \cdot g^{-1}$)
AC0.5_500	13.18	0.03	2.80	30.01
AC1.0_500	29.06	0.04	2.40	70.03
AC0.5_600	451.20	0.16	2.40	100.14
AC1.0_600	470.61	0.27	2.40	140.87
B_AC0.5_500	4.25	0.02	5.30	40.35
B_AC1.0_500	5.74	0.03	5.20	140.85
B_AC0.5_600	286.92	0.12	4.30	245.36
B_AC1.0_600	305.68	0.16	3.90	273.25

The XRD patterns of AC1.0_600 and B_AC1.0_600 displayed in Fig. 2c show diffraction peaks at 2θ. Because activated carbon lacks a well-defined crystalline structure, its XRD pattern typically shows a broad peak centered around 2θ values of about 20–30 degrees. This broad peak is characteristic of disordered or amorphous carbon. As seen in Fig. 3c, the XRD patterns of AC1.0_600 and B_AC1.0_600 appear at around 24° and 43°, respectively, corresponding to the graphitic-like structure of activated carbon, indicating a certain

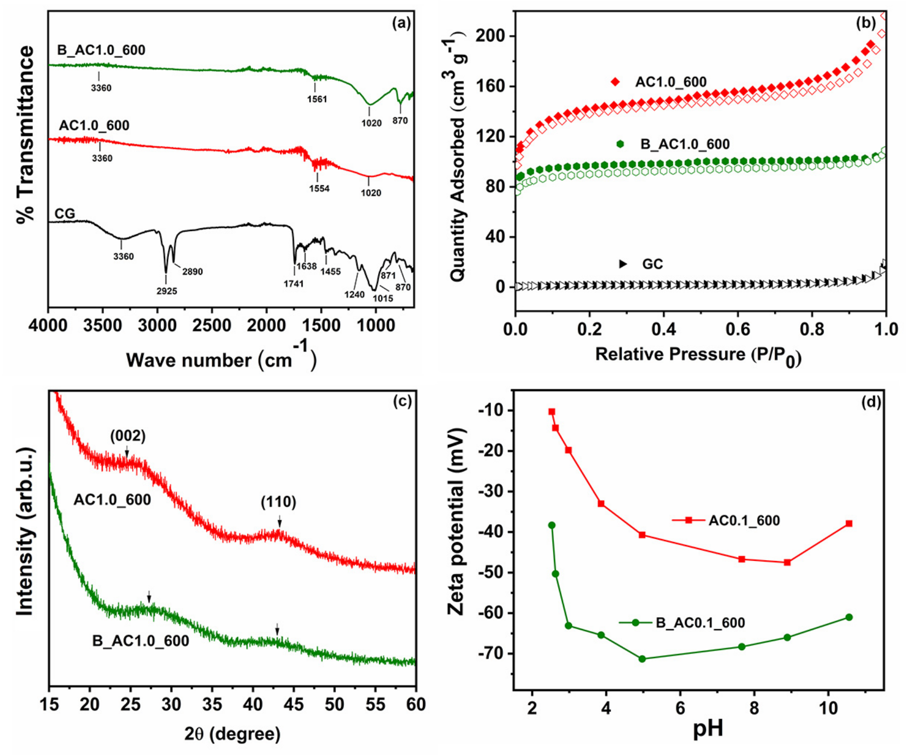

Fig. 2 (a) FTIR spectra of coffee grounds (CG), coffee ground activated carbon (AC1.0_600), and boric acid-doped coffee ground activated carbon (B_1.0AC_600), (b) Nitrogen adsorption-desorption isotherm plot, (c) XRD pattern, and (d) zeta potential of AC1.0_600 and B_1.0AC_600 samples.

degree of graphitization that confers good electrical conductivity.

Surface potential is a crucial parameter for investigating the interaction between 2 surfaces. The charge on the AC surface plays a key role in promoting affinity between the material surface and electrolyte ions during the charging/discharging process, essential for achieving improved electrochemical performance [28]. In this study, AC surface potential was determined through zeta potential measurements, as detailed in Fig. 2d. The zeta potential of boric acid-doped activated carbon (B_AC1.0_600) was slightly more negative than that of the undoped sample, indicating successful incorporation of oxygen (O) atom with electron-withdrawing activity and boron (B) atom with electron-donating activity. Following the modifications, the increase in the negative value of the zeta potential reveals the inclusion of negatively charged surface groups [19]. The conductivity capacity was influenced by the zeta potential of the carbon electrode, providing a possible explanation for enhanced electrostatic attraction with cations.

Based on several successful studies on activated carbon (AC), it has been noted that its surface area and porous structure can vary widely, influenced by factors such as activator concentration [29], activation temperature [30], type of activator [31], and biomass type [32].

Performance of AC and B_AC as electrodes

Cyclic voltametric (CV) analysis

The effect of activation temperature and activating ratio on preparing AC from coffee grounds is considered the prime factor to optimize the for-electrode preparation. Based on preliminary experiments, 500 °C and 600 °C were selected as the optimal carbonization temperatures. Carbonization at 400 °C resulted in insufficient activation, leading to lower porosity and reduced electrochemical performance. Conversely, excessive burn-off occurred at 700 °C, which reduced the yield and specific surface area. Therefore, 500 °C and 600 °C were chosen to achieve a balance between yield, surface area, and pore structure, ensuring enhanced electrochemical properties. Optimizing AC electrode preparation involves adjusting activation temperature (500 °C and 600 °C) and AC:KOH mass ratios (0.5:1.0 and 1.0:1.0), denoted as AC0.5_500, AC1.0_500, AC0.5_600, and AC1.0_600. As seen in Fig. 3a, by increasing the carbonization temperature, the specific surface area of ACs increased. Despite the highest specific surface area among all samples,

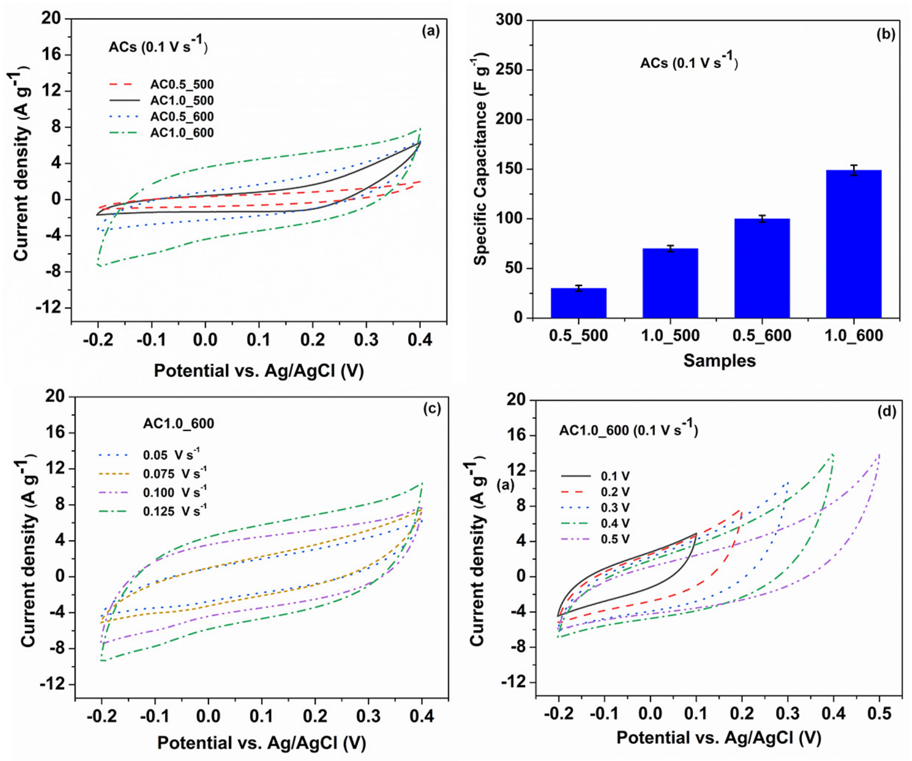

Fig. 3 Effects of temperature and activation content on (a) Cyclic voltammetry (CV) profile and (b) specific capacitance (C_p) values of AC electrodes, (c) effect of scan rate, and (d) effect of window volt on CV profile of AC1.0_600 electrode.

AC1.0_600 had the highest C_p values (160 $\text{F}\cdot\text{g}^{-1}$), which was due to its highest pore volume and SSA. This suggests that, in addition to the surface area, the micropore and mesopores also play an essential role in enhancing the C_p of ACs. The maximum current value of CV profile was observed in AC1.0_600 sample followed by AC0.5_600. The finding result indicates that the electrochemical reaction of the AC1.0_600 sample is highest. The reason could be from surface area and pore sites in activated carbon that serve as adsorption sites and ion transport channels, crucial for supercapacitor performance. Achieving optimal capacitance relies on the balanced distribution of surface area and pore volume in the activated carbon electrode. Additionally, surface oxygen content enhances activated carbon wettability and contributes to pseudo-capacitance [33]. High-temperature carbonization and an appropriate alkali-to-biomass ratio are employed to synthesize activated carbons with suitable pore structures and SSA, especially for high-performance supercapacitors. The creation of pore structures and surface properties in activated carbon depends on the synergistic effects of the production process, significantly influencing the electrochemical performance. Furthermore, the total area under the CV curve corresponds to the total charge associated with the electrochemical process. It can be used to quantify the capacitive performance of electrode. The specific capacitance (C_p) is calculated from CV curves using the equation [10, 34],

$$C_p = \frac{I}{ms} \tag{1}$$

where C_p is the specific capacitance, I is the average of anodic/cathodic current (A), s is the scan rate ($\text{V}\cdot\text{s}^{-1}$), and m is the mass of electrode material (g). The specific capacitance values, depicting the influence of activation temperature on the conductibility of activated carbon material, are shown in Fig. 3b. Values deduced from CV analysis are 30, 70, 100, and 160 $\text{F}\cdot\text{g}^{-1}$ for AC0.5_500, AC1.0_500, AC0.5_600, and AC1.0_600, respectively. Among the different temperature and activating content samples, higher pore volume contributes to elevated specific capacitance values, with AC1.0_600 exhibiting a particularly high pore volume and, consequently, higher electrochemical behaviors. The specific capacitance achieved in this work is higher than the values reported earlier for activated carbon [10]. A notable relationship is observed between capacitance value and activation temperature as well as the chemical activation ratio of carbon materials. At a higher activation temperature (600 °C), the specific capacitance value of AC1.0_600 (149 $\text{F}\cdot\text{g}^{-1}$) is much higher than that of AC1.0_500 and AC0.5_600

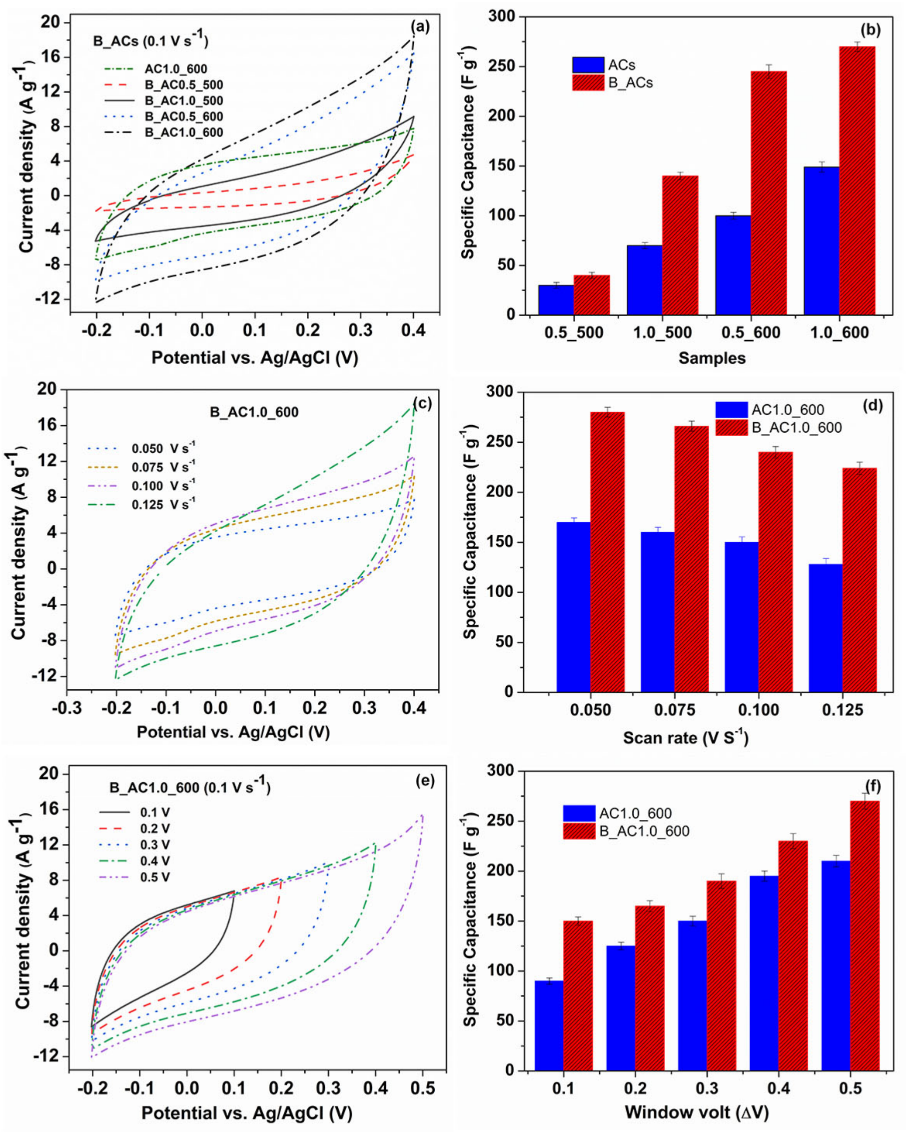

Fig. 4 (a) CV profile of AC1.0_600 and B_AC electrodes and (b) C_p values of AC and B_AC electrodes together with effect of scan rate on (c) CV profile and (d) C_p values, and effect of window volt on (e) CV profile and (f) C_p values of B_AC1.0_600 electrode.

(70 and 100 $\mathrm{F \cdot g^{-1}}$, respectively). Similarly, AC1.0s, with a higher KOH ratio, deliver the highest specific capacitance. Therefore, the carbonization condition of a 1:1 mass ratio at 600 °C (AC1.0_600) is selected for effect of scan rate and window volt studies.

The effect of scan rate and window volt on CV profile of selected AC1.0_600 electrode was examined. Fig. 3c exhibits cyclic voltammogram variation in scan rate from 0.05 $\mathrm{V \cdot s^{-1}}$ to 0.125 $\mathrm{V \cdot s^{-1}}$, and Fig. 3d exhibits window voltage from 0.1 V to 0.5 V in a 6 M KOH electrolyte of the AC1.0_600 electrode. In Fig. 3c, the CV profile shows the maximum current value at a higher scan rate. However, the power rate capability of AC1.0_600 is optimal at 0.1 $\mathrm{V \cdot s^{-1}}$ and a window voltage of 0.4 V because it maintains a quasi-rectangular shape, in contrast to poor cyclability evident in leaf-like cyclic voltammograms at higher scan rates and window voltages. The increase in capacitance at low scan rates for AC1.0_600 electrodes can be attributed to the electrode surface becoming more accessible to many electrolyte ions as the scan rate decreases. This allows for the full utilization of the electrode surface at lower scan rates.

The impact of doping boric acid (B_AC0.1_600) molecule into the activated carbon matrix on capacitive performance was assessed through cyclic voltammetry plots using a consistent scan rate (0.1 $\mathrm{V \cdot s^{-1}}$), as shown in Fig. 4a. The capacitive performance of boron-doping significantly surpassed that of the undoped AC1.0_600. The influence of temperature (500 °C and 600 °C) and chemical activation ratio (0.5:1.0 and 1.0:1.0) on the doping of boric acid was also studied, denoted as B_AC0.5_500, B_AC1.0_500, B_AC0.5_600, and B_AC1.0_600. Similar to the undoped case, doping boric acid with a higher activation temperature (600 °C) and higher KOH ratio delivers the maximum current value (Fig. 4a) and highest specific capacitance (Fig. 4b). Therefore, the carbonization condition of a 1:1 mass ratio at 600 °C (B_AC1.0_600) is selected for further studies. Specific capacitance values derived from CV analysis for AC1.0_600 and B_AC1.0_600 are 149 and 270 $\mathrm{F \cdot g^{-1}}$, respectively, as illustrated in Fig. 5b. However, not only surface area/pore volume but also functional groups produced on the activated carbon surface influence the capacitance value of the carbon electrode material. Despite AC1.0_600 having higher pore volume and surface area (0.27 $\mathrm{cm^3 \cdot g^{-1}}$ and 470.61 $\mathrm{m^2 \cdot g^{-1}}$, respectively), its specific capacitance value is considerably lower than that of B_AC1.0_600. Interestingly, among the different temperatures and activating contents in both doping and undoping samples, higher temperature and KOH content that induce higher pore volume/functional groups contribute to elevated specific capacitance values, with B_AC1.0_600 exhibiting a particularly high surface area/pore volume and functional groups, consequently, superior electrochemical behaviors.

Fig. 4c,d exhibit the cyclic voltammogram and capacitance value variation at different scan rates from 0.05 $\mathrm{V \cdot s^{-1}}$ to 0.125 $\mathrm{V \cdot s^{-1}}$, while Fig. 4e,f display the cyclic voltammogram and capacitance value at different window voltages from 0.1 V to 0.5 V in a 1 M KOH electrolyte of the B_AC1.0_600 electrode. In Fig. 4c, the CV profile shows the maximum current value at a higher scan rate. As expected, the capacitance value decreases with the scan rate, as the diffusion of ions inside the inner pores of the carbon electrode is restricted at a higher scan rate, as shown in Fig. 4d. The power rate capability of B_AC1.0_600 is optimal at 0.1 $\mathrm{V \cdot s^{-1}}$ and a window voltage of 0.4 V (Fig. 4e,f) because it maintains a quasi-rectangular shape, highlighting the primary EDL capacitance behavior [35] and contrasting with poor cyclability evident in leaf-like cyclic voltammograms at higher scan rates.

Galvanostatic charge/discharge (GCD) analysis

GCD is an important and commonly used technique. It is usually distinguishing the principal charge storage mechanism, whether adsorption/desorption or pseudo-capacitive supercapacitor. The GCD curves of symmetric capacitors consisting of AC1.0_600 and B_AC1.0_600 employing 1 M KOH electrolyte under different current densities at 0.5–1.25 $\mathrm{A \cdot g^{-1}}$ are depicted in Fig. 5a,b. While the specific capacitance, an energy density, and power density values calculated from GCD curves of corresponding both electrode materials are depicted in Fig. 5c–e, respectively. The GCD curves of AC1.0_600 and B_AC1.0_600 are not a perfect triangle shape, indicating that the charge storage is contributed by both EDLC and pseudocapacitance mechanisms [24].

The specific capacitance (C_p, $\mathrm{F \cdot g^{-1}}$), energy density (E, $\mathrm{Wh \cdot kg^{-1}}$), and power density ($P$, $\mathrm{W \cdot kg^{-1}}$) of B_AC1.0_600 can be calculated by using the following equations:

$$C_p = \frac{I\,\Delta t}{m\,\Delta V} \tag{2}$$

$$E = \frac{C_p\,\Delta V^2}{2\times 3.6} \tag{3}$$

$$P = \frac{E}{\Delta t} \tag{4}$$

where C_p represents the specific capacitance ($\mathrm{F \cdot g^{-1}}$) of the electrode materials, I (A) is the discharge current, Δt (s) is the discharge time, m (g) is the mass of the ACs on the electrode, and ΔV (V) represents the working voltage.

The specific capacitance is lower when increasing the current density as displayed in Fig. 5c. The C_p value decreases with increasing current density. For example, as the current density rises from 0.5 $\mathrm{A \cdot g^{-1}}$ to 1.25 $\mathrm{A \cdot g^{-1}}$, C_p decreases from 146.25 $\mathrm{F \cdot g^{-1}}$ to 22.06 $\mathrm{F \cdot g^{-1}}$ for the AC1.0_600 electrode and from 282.43 $\mathrm{F \cdot g^{-1}}$ to 83.13 $\mathrm{F \cdot g^{-1}}$ for the B_AC1.0_600 electrode. This decrease in C_p value may be attributed to the reduced ability of electrolyte ions to diffuse rapidly through the electrode/KOH solution interface and the slow rate of their interaction with the electrode surface at high applied current density [23]. Therefore, the synthesized material demonstrates efficient electrochemical energy storage at slow scan rates. Results indicated that the B_AC1.0_600 electrode exhibited significantly higher electric current compared to A1.0_600 electrodes. The B_AC1.0_600 electrode, modified with boric acid, demonstrated the highest specific capacitance of approximately 282 $\mathrm{F \cdot g^{-1}}$, 2-fold higher than that of unmodified material (146.25 $\mathrm{F \cdot g^{-1}}$) at a current density of 0.5 $\mathrm{A \cdot g^{-1}}$.

At low current densities, the GCD curves of AC1.0_600 and B_AC1.0_600 in Fig. 5a,b slightly deviate from ideal isosceles triangle shapes, indicating highly reversible charge-discharge processes [33, 35]. B_AC1.0_600 exhibits a longer discharge time at 0.5 $\mathrm{A \cdot g^{-1}}$ and a 193% higher specific capacitance compared to AC1.0_600, attributed to factors such as pHpzc and surface boron and oxygen content. Despite B_AC1.0_600 having lower SSA and pore volume, its higher specific capacitance suggests elevated boron and oxygen contents and a less negative

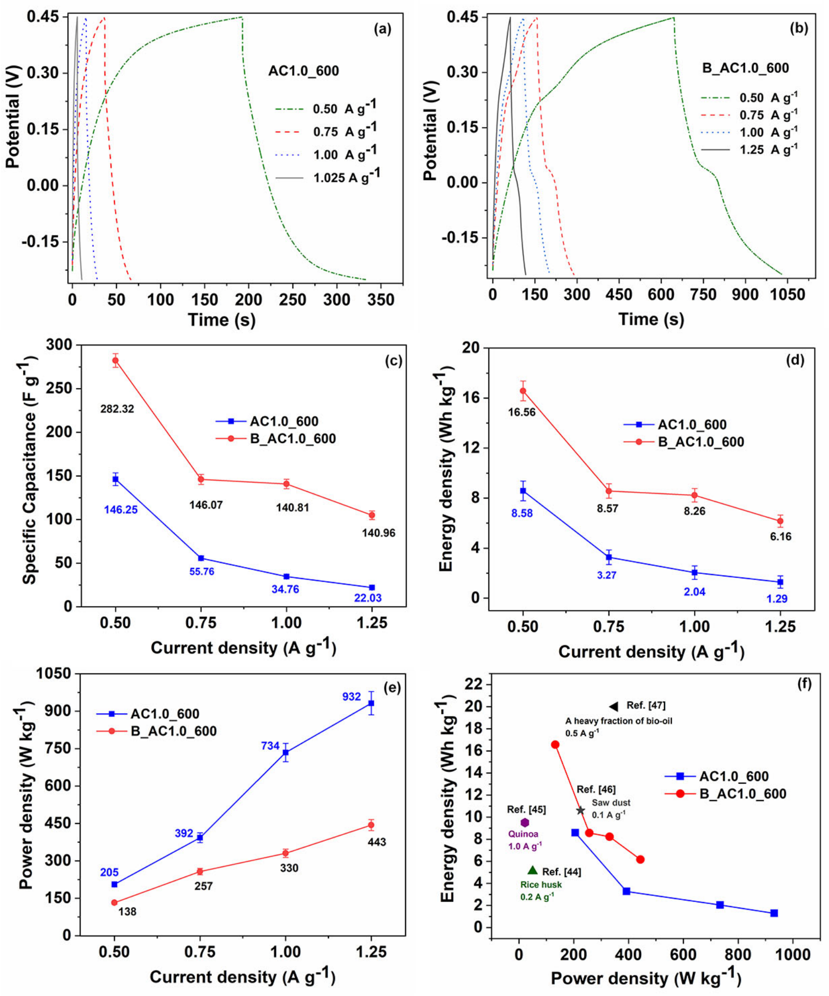

Fig. 5 Effect of current density on the galvanostatic charge-discharge (GCD) profiles of (a) AC1.0_600 and (b) B_AC1.0_600, (c) specific capacitance (C_p) values, (d) energy density, and (e) power density of both electrodes, along with (f) Ragone plots compared with previous studies [39, 40].

Table 3 The comparison between the tested electrodes in KOH electrolyte with other similar reported biomass derived carbon or composite with supercapacitor parameters.

Biomass derived carbon	Activating agent	Heteroatom	Electrolyte	Tested condition	C_p ($\mathrm{F \cdot g^{-1}}$)	Ref.
Coffee ground	KOH	–	1 M H_2SO_4	5 $\mathrm{mV \cdot s^{-1}}$	205	[8]
Coffee ground	KOH	–	2 M KOH	0.5 $\mathrm{A \cdot g^{-1}}$	105	[14]
Coffee ground	Thermal 600	O, N	5 M KOH	5 $\mathrm{mV \cdot s^{-1}}$	190	[16]
Waste tire	KOH	B, O	2 M $ZnSO_4$	1 $\mathrm{A \cdot g^{-1}}$	230	[24]
Corn husk	K_2CO_3	O, N and S	0.5 M H_2SO_4	5 $\mathrm{mV \cdot s^{-1}}$	269	[5]
Soybean root	KOH	N	6 M KOH	0.5 $\mathrm{A \cdot g^{-1}}$	276.0	[36]
Broad bean	KOH	N, S	1 M H_2SO_4	0.5 $\mathrm{A \cdot g^{-1}}$	229.0	[37]
Soybean pod	KOH	O, N, P	6 M KOH	1 $\mathrm{A \cdot g^{-1}}$	321.0	[38]
Coffee ground	KOH	B, O	1 M KOH	0.5 $\mathrm{A \cdot g^{-1}}$	282	This study

pHpzc value. This discrepancy may be due to increased pseudo-capacitance from boron and enhanced electrolyte ion diffusion facilitated by interactions of oxygen-containing groups. These findings suggest that porous carbons derived from waste coffee grounds and modified with boric acid hold significant potential as alternative electrode materials for supercapacitors.

The overall performance of carbon-based electrode materials is influenced by various parameters, including electrical conductivity, pore size distribution, and the method of electrode formation. A comparison of the tested electrodes with other similar biomass-derived carbons or composites with supercapacitor parameters is provided in Table 3. Utilizing essentially cost-free biomass waste as a precursor offers a clear advantage for synthesizing high surface area carbons, facilitating practical applications in energy storage.

Furthermore, the B_AC1.0_600 electrode demonstrated an energy density of 16.54 $\mathrm{Wh \cdot kg^{-1}}$ and a power density of 138.54 $\mathrm{W \cdot kg^{-1}}$ at 0.5 $\mathrm{A \cdot g^{-1}}$. Energy density and power density values were plotted in Fig. 5d,e, respectively. When comparing the electrochemical performance with previously reported materials [14, 36–38], the results demonstrate that the boric acid-doped samples exhibit competitive energy and power densities, affirming their potential as electrode materials for supercapacitors. The Ragone plot, illustrated in Fig. 5f, compares the energy density and power density of the nitrogen-modified activated carbon electrodes developed in this study with those reported in previous works. Compared to other studies, including those by [39, 40], the nitrogen-modified activated carbon in this research demonstrates higher energy densities at similar power levels. This result underscores the effectiveness of the surface modification approach, particularly the introduction of nitrogen functional groups, which enhances the conductivity of the material.

CONCLUSION

This study aimed to produce activated carbon from coffee grounds (CGAC) using KOH as an activator and subsequently modify the CGAC sample with boric acid to form supercapacitor electrodes. The results show that AC0.5_500, AC1.0_500, AC0.5_600, and AC1.0_600 displayed a well-distributed pore structure, optimal yield percentage, and the high surface area. Consequently, these samples underwent surface treatment with boric acid at 140 °C for 48 h via hydrothermal. The electrocapacitive behavior of both modified and unmodified activated carbon was investigated through CV and GCD techniques. Electrocapacitive behavior reveals that higher temperatures and KOH content induced higher specific capacitance values. The boric acid-modified CGAC electrode exhibited significantly higher electric current compared to bare pencil graphite and other sample electrodes. The B_AC1.0_600 electrode, modified with boric acid, demonstrated the highest specific capacitance. These findings suggest that porous CGAC and modified with boric acid hold significant potential as alternative electrode materials for supercapacitors.

Acknowledgements: This work was supported by National Higher Education, Science, Research and Innovation Policy Council, Thaksin University (Fundamental Research Fund; TSU-66A105000013) Fiscal Year 2023. The authors would like to thank the Department of Chemistry, Faculty of Science and innovation digital, Thaksin University, for providing research facilities.

REFERENCES

1. Temesgen T, Bekele ET, Gonfa BA, Tufa LT, Sabir FK, Tadesse S, Dessie Y (2023) Advancements in biomass derived porous carbon materials and their surface influence effect on electrode electrochemical performance for sustainable supercapacitors: A review. *J Energy Storage* **73**, 109293.
2. Wang S, Ren Z, Li J, Ren Y, Zhao L, Yu J (2014) Cotton-based hollow carbon fibers with high specific surface area prepared by ammonia etching for supercapacitor application. *RSC Adv* **4**, 31300–31307.
3. Kraiwattanawong K (2022) A review on the development of a porous carbon-based as modeling materials for electric double layer capacitors. *Arab J Chem* **15**, 103625.
4. Jain A, Michalska M, Zaszczyńska A, Denis P (2022) Surface modification of activated carbon with silver nanoparticles for electrochemical double layer capacitors. *J Energy Storage* **54**, 105367.
5. Lobato-Peralta DR, Duque-Brito E, Orugba HO, Arias DM, Cuentas-Gallegos AK, Okolie JA, Okoye PU (2023) Sponge-like nanoporous activated carbon from corn husk as a sustainable and highly stable supercapacitor electrode for energy storage. *Diam Relat Mater* **138**, 110176.
6. Thungsuai K, Pimpha N, Chaleawlert-umpon S (2023) The role of carbon electrode parameters on capacitive deionization efficiency. *ScienceAsia* **49**, 859–863.
7. Li M, Xiao H, Zhang T, Li Q, Zhao Y (2019) Activated carbon fiber derived from sisal with large specific surface area for high-performance supercapacitors. *ACS Sustain Chem Eng* **7**, 4716–4723.
8. Padilla-Martínez ED, Pérez-Buendía SK, López-Sandoval R, Sánchez-Rodríguez CE (2023) Electrochemical energy storage from spent coffee grounds-derived carbon by KOH activation. *J Energy Storage* **71**, 108115.
9. Huang P, Chen F, Zheng M, Xiao Y, Hu H, Liang Y, Liu Y, Dong H (2024) Comparison of porous carbon prepared by conventional and microwave-assisted hydrothermal carbonization and its application in supercapacitors. *J Appl Electrochem* **54**, 2205–2218.
10. Surya K, Michael MS (2021) Hierarchical porous activated carbon prepared from biowaste of lemon peel for electrochemical double layer capacitors. *Biomass Bioenergy* **152**, 106175.
11. Kongsune P, Rattanapan S, Chanajaree R (2021) The removal of $\mathrm{Pb^{2+}}$ from aqueous solution using mangosteen peel activated carbon: Isotherm, kinetic, thermodynamic and binding energy calculation. *Groundw Sustain Dev* **12**, 100524.
12. Rattanaphan S, Rungrotmongkol T, Kongsune P (2020) Biogas improving by adsorption of $\mathrm{CO_2}$ on modified waste tea activated carbon. *Renew Energy* **145**, 622–631.
13. Wang L, Feng X, Li X, Ma H, Wu J, Chen Y, Zhou J (2022) Valorization of lignin: Application of lignin-derived activated carbon in capacitors and investigation of its textural properties and electrochemical performance. *Diam Relat Mater* **122**, 108791.

14. Chiu Y-H, Lin L-Y (2019) Effect of activating agents for producing activated carbon using a facile one-step synthesis with waste coffee grounds for symmetric supercapacitors. *J Taiwan Inst Chem Eng* **101**, 177–185.
15. Hamza L, Khelifi A, Trari M, Addoun A (2017) Synthesis and characterization of microporous activated carbon from coffee grounds using potassium hydroxides. *J Clean Prod* **147**, 254–262.
16. Hamza L, Khelifi A, Trari M, Addoun A (2021) *In-situ* O/N-heteroatom enriched activated carbon by sustainable thermal transformation of waste coffee grounds for supercapacitor material. *J Energy Storage* **33**, 102113.
17. He H, Zhang Y, Wang P, Hu D (2021) Preparation of sponge-cake-like N-doped porous carbon materials derived from silk fibroin by chemical activation. *Microporous Mesoporous Mater* **317**, 110998.
18. Rufford TE, Hulicova-Jurcakova D, Fiset E, Zhu Z, Lu GQ (2009) Double-layer capacitance of waste coffee ground activated carbons in an organic electrolyte. *Electrochem Commun* **11**, 974–977.
19. Hegazy MA, Mohammedy MM, Dhmees AS (2021) Phosphorous and sulfur doped asphaltene derived activated carbon for supercapacitor application. *J Energy Storage* **44**, 103331.
20. Cheng L, Wu J (2021) N-doped carbon derived from regeneration nylon 6 used as an electroactive material for electrochemical capacitor. *Diam Relat Mater* **115**, 108356.
21. Govindarasu KG, Venkatesan R, Rajagopal RK, Rajamanickam G, Arumugam P (2023) Enhanced electrochemical performances of three-dimensional cubic ordered mesoporous carbon by boron-doping for supercapacitor applications. *J Appl Electrochem* **53**, 1111–1124.
22. Jaouadi M, Marzouki M, Hamzaoui AH, Ghodbane O (2022) Enhanced electrochemical performance of olive stones-derived activated carbon by silica coating for supercapacitor applications. *J Appl Electrochem* **52**, 125–137.
23. Ning K, Zhao G, Liu H, Hu M, Huang F, Li H, Zhang L, Zhu G, et al (2022) N and S co-doped 3D hierarchical porous carbon as high-performance electrode material for supercapacitors. *Diam Relat Mater* **126**, 109080.
24. Li J, Sun Y, Jia X, Chen Y, Tang Y, Wan P, Pan J (2024) Boron, oxygen co-doped porous carbon derived from waste tires with enhanced hydrophilic interface as sustainably high-performance material for supercapacitors. *J Energy Storage* **80**, 110320.
25. Li K, Li P, Sun Z, Shi J, Huang M, Chen J, Liu S, Shi Z, et al (2023) All-cellulose-based quasi-solid-state supercapacitor with nitrogen and boron dual-doped carbon electrodes exhibiting high energy density and excellent cyclic stability. *Green Energy Environ* **8**, 1091–1101.
26. Romanos J, Beckner M, Stalla D, Tekeei A, Suppes G, Jalisatgi S, Lee M, Hawthorne F, et al (2013) Infrared study of boron-carbon chemical bonds in boron-doped activated carbon. *Carbon* **54**, 208–214.
27. Shen F, Zhu H, Luo W, Wan J, Zhou L, Dai J, Zhao B, Han X, et al (2015) Chemically crushed wood cellulose fiber towards high-performance sodium-Ion batteries. *ACS Appl Mater Interfaces* **7**, 23291–23296.
28. Ng SH, Vix-Guterl C, Bernardo P, Tran N, Ufheil J, Buqa H, Dentzer J, Gadiou R, et al (2009) Correlations between surface properties of graphite and the first cycle specific charge loss in lithium-ion batteries. *Carbon* **47**, 705–712.
29. Qie Z, Zhang X, Wang Z, Liu Z, Alhassawi H, Li H, Chen G, Zhao G (2024) Effect of pretreatment and activation conditions on pore development of coal-based activated carbon. *J Ind Eng Chem* **139**, 611–619.
30. Chen J, Liu Y, Liu J, Duan Q, Wang Z, Song J, Ji C, Sun J (2024) Effects of carbonization on the structure and sorption properties of coffee grounds for Pb(II) and Ni(II) in various metal systems. *Desalination Water Treat* **320**, 100623.
31. Quan C, Miskolczi N, Feng S, Grammelis P, Wu C, Gao N (2023) Effect of type of activating agent on properties of activated carbon prepared from digested solid waste. *J Environ Manage* **348**, 119234.
32. Jiao H, Guo X, Shu F, Zhang Q, Wu W, Jin Y, Jiang B (2025) Structure-property-function relationships of wood-based activated carbon in energy and environment materials. *Separation and Purification Technology* **353**, 128607.
33. Song M, Zhou Y, Ren X, Wan J, Du Y, Wu G, Ma F (2019) Biowaste-based porous carbon for supercapacitor: The influence of preparation processes on structure and performance. *J Colloid Interface Sci* **535**, 276–286.
34. Conway BE (2013) *Electrochemical Supercapacitors: Scientific Fundamentals and Technological Applications*, Springer Science & Business Media.
35. Qin Q, Wang J, Tang Z, Jiang Y, Wang L (2024) Mesoporous activated carbon for supercapacitors derived from coconut fiber by combining H_3PO_4-assisted hydrothermal pretreatment with KOH activation. *Ind Crops Prod* **208**, 117878.
36. Guo N, Li M, Wang Y, Sun X, Wang F, Yang R (2016) Soybean root-derived hierarchical porous carbon as electrode material for high-performance supercapacitors in ionic liquids. *ACS Appl Mater Interfaces* **8**, 33626–33634.
37. Xu G, Han J, Ding B, Nie P, Pan J, Dou H, Li H, Zhang X (2015) Biomass-derived porous carbon materials with sulfur and nitrogen dual-doping for energy storage. *Green Chem* **17**, 1668–1674.
38. Liu Z, Zhu Z, Dai J, Yan Y (2018) Waste biomass based-activated carbons derived from soybean pods as electrode materials for high-performance supercapacitors. *ChemistrySelect* **3**, 5726–5732.
39. Liu Y, Tan H, Tan Z, Cheng X (2022) Rice husk derived capacitive carbon prepared by one-step molten salt carbonization for supercapacitors. *J Energy Storage* **55**, 105437.
40. Jiang H, Liu L, Zhao K, Liu Z, Zhang X, Hu S (2020) Effect of pyridinic- and pyrrolic-nitrogen on electrochemical performance of Pd for formic acid electrooxidation. *Electrochim Acta* **337**, 135758.